Materials Advances

ROYAL SOCIETY OF CHEMISTRY

PAPER

View Article Online
View Journal | View Issue

Cite this: *Mater. Adv.*, 2026, 7, 4797

Designing a nanostructured Biginelli reaction-based dipodal receptor for effective corrosion control of mild steel in 1 M H_2SO_4

Amisha Yadav,[a] Jasdeep Kaur,[b] Amanpreet Singh, *[b] Ankush Kumar Tangra *[c] and Gurjaspreet Singh [d]

A novel nanostructured dipodal receptor synthesized *via* a one pot Biginelli multicomponent reaction was successfully engineered into organic nanoparticles (ONPs) and evaluated as an efficient corrosion inhibitor for mild steel in 1 M H_2SO_4. The rational molecular design, incorporation of multiple electron donating heteroatoms (N and O) and conjugated π-system facilitate strong adsorption onto the steel surface and promote the formation of a compact protective film. Electrochemical and gravimetric analysis confirmed excellent inhibition performance, achieving efficiencies of 90.14% (weight loss), 91.36% (potentiodynamic polarization), and 97.50% (electrochemical impedance spectroscopy) at an optimal concentration of 20 mg L^{-1}. Polarisation studies demonstrated mixed type inhibition behaviour with predominant control over acid dissolution, while impedance results revealed a significant increase in charge transfer resistance and reduced double layer capacitance, strengthening the formation of an effective adsorption barrier. The superior inhibition efficiency at low concentration highlights the synergic effect of the dipodal architecture and nanoscale dimensions, offering a scalable and high-performance strategy for acid corrosion mitigation in industrial systems.

Received 9th December 2025,
Accepted 18th March 2026

DOI: 10.1039/d5ma01432h

rsc.li/materials-advances

1. Introduction

Heterocyclic compounds (HCs) represent a fundamental class of organic molecules, widely found in both natural and synthetic systems.[1] They serve as the core structure in numerous biologically active substances, including hormones, nucleic acids, and vitamins.[2,3] Owing to their chemical versatility and biological relevance, HCs have become essential in various fields, such as agrochemicals,[4] materials science, synthetic dyes, and pharmaceuticals.[5] These compounds are particularly valuable in medicinal chemistry due to their ability to engage in hydrogen bonding,[6] π–π stacking, and other non-covalent interactions with biological targets.[7] As a result, many heterocycles possess a wide range of therapeutic properties, including antibacterial,[8] anti-inflammatory,[9] antioxidant,[10] antidiabetic,[11] antifungal,[12] and anticonvulsant activities. Among the many types of heterocyclic scaffolds, Biginelli reaction-based heterocycles have garnered significant attention. These molecules are widely used in the development of calcium channel blockers[13] and antihypertensive agents,[14] making their synthesis a key area of ongoing pharmaceutical research. The ability to incorporate such biologically active frameworks into novel materials—such as organic nanoparticles—opens new avenues for applications beyond medicine, including advanced corrosion protection.[15]

The Biginelli reaction is a renowned three-component reaction used to fabricate 3,4-dihydropyrimidin-2(1*H*)-ones (DHPMs),[16] a class of heterocyclic compounds with diverse biological and material applications. Biginelli-derived compounds have found widespread use in drug delivery systems, chemical sensing, and as potential anticancer, antiviral, and anti-inflammatory agents.[17–19] Their presence in pharmaceutical and medicinal chemistry is well-documented due to their broad-spectrum biological activity and synthetic accessibility. The Biginelli reaction is a classic example of a multicomponent reaction (MCR)—a type of chemical transformation where three or more than three reactants come together in a single reaction step to form a final product, typically deprived of the need to isolate or purify intermediate compounds.[20] This one-pot strategy offers an efficient and streamlined approach to synthesizing complex molecules. MCRs are highly valued in modern synthetic chemistry due to their remarkable synthetic efficiency, high atom economy, operational simplicity and compatibility with mild

[a] *Department of Chemistry, UIS, Chandigarh University, Mohali, Punjab, India*
[b] *Department of Chemistry, Bahra Research Innovation & Knowledge Cluster, Rayat Bahra University, Chandigarh-Ropar NH 205, Greater Mohali, Punjab, 140103, India. E-mail: amanchem15@gmail.com*
[c] *Department of Physics, Bahra Research Innovation & Knowledge Cluster, Rayat Bahra University, Chandigarh-Ropar NH 205, Greater Mohali, Punjab, 140103, India. E-mail: aktangra@gmail.com*
[d] *Department of Chemistry, Panjab University, Chandigarh, 160014, India*

reaction conditions.[21–24] MCRs are well-suited for organic synthesis, materials science, and molecular diversification. These reactions offer exceptional structural diversity, allowing precise incorporation of functional groups such as electron-rich heteroatoms and conjugated π-systems within the single molecular framework. Such features are particularly advantageous in rational design of functional materials, where the molecular architecture significantly influences the performance. The rapid construction of Biginelli-based heterocyclic scaffolds through MCR strategies provides a versatile platform not only for pharmaceutical and functional material development but also for engineering advanced materials for enhanced adsorption and corrosion inhibition.

Mild steel is one of the most frequently used construction and engineering materials across a variety of industries, particularly in the chemical, petroleum, and construction sectors. These industries frequently utilize acids for processes such as descaling, cleaning, and pickling, which unfortunately accelerate the corrosion of mild steel. This acid-induced degradation compromises structural integrity and leads to significant safety risks, material degradation, and financial losses due to equipment failure and increased maintenance demands. Consequently, the development of efficient, stable, and scalable corrosion inhibitors capable of protecting mild steel under harsh acidic conditions is of critical industrial and environmental importance.

Recent advancements in corrosion science have focused on developing synthetic corrosion inhibitors, particularly through multicomponent reactions (MCRs). Heterocyclic compounds generated *via* MCRs are especially promising as inhibitors due to the existence of electron-rich heteroatoms (such as N, O, and S) and conjugated π-systems, which promote strong adsorption onto metal surfaces and the formation of protective layers. While plant-based corrosion inhibitors—derived from natural extracts—have attracted interest for their eco-friendly and cost-effective nature, they suffer from several drawbacks. These include inconsistent chemical composition, limited stability under aggressive industrial conditions, and slower inhibition kinetics, all of which hinder their widespread application.[25–31]

Despite these advances, the rational design of Biginelli reaction derived frameworks as nanostructured dipodal receptors for corrosion inhibition remains largely unexplored. In particular, the combined strategy of exploiting dipodal molecular architecture providing dual anchoring sites and nanoscale structuring to enhance adsorption efficiency and surface coverage has not been systematically investigated. This approach is expected to improve molecular interaction with the metal surface, strengthen adsorption stability and facilitate the formation of a compact and uniform protective film. Therefore, integrating MCR chemistry with nanoengineering represents a promising yet underdeveloped direction in the area of corrosion inhibitor design. In this study, we report the synthesis of a dipodal Biginelli-based receptor *via* a one-pot multicomponent reaction. The resulting compound was further processed into organic nanoparticles (ONPs) to enhance its dispersion and applicability in aqueous media. The corrosion inhibition potential of the fabricated ONPs was then evaluated in 1 M sulfuric acid, demonstrating their potential as a robust, efficient, and scalable alternative to conventional corrosion inhibitors.

2. General experimental

All reagents and solvents employed in the synthesis were of analytical or reagent grade. They were used without further purification. Terephthaldehyde (purity: 99%), ethyl acetoacetate (≥99.0%, GC), 2-aminobenzimidazole (97%), and zinc perchlorate were purchased from Sigma-Aldrich. Solvents such as methanol (≥99.9%, GC, reagent grade) and dimethyl sulfoxide (DMSO) (99.9%) were obtained from Avra Synthesis.

The synthesized dipodal Biginelli-based receptor was characterized using proton nuclear magnetic resonance NMR spectroscopy on a JEOL NMR spectrometer, with tetramethylsilane (TMS) as an internal reference.

2.1. Preparation of organic nanoparticles (ONPs) and dipodal receptor 4

The dipodal receptor 4 was prepared through a one-pot Biginelli condensation involving terephthaldehyde (TPA) (1), ethyl acetoacetate (EAA) (2), and 2-aminobenzimidazole (2-ABI) (3). In a standard procedure, 0.150 g (0.001 mmol) of TPA, 0.26 mL (0.002 mmol) of EAA, and 0.297 g (0.002 mmol) of 2-ABI were dissolved in methanol within a round-bottom flask. Zinc perchlorate (10 mol%) was then introduced as a catalyst. The reaction mixture was refluxed in an oil bath with continuous stirring for 3–4 hours. Progress of the reaction was tracked using thin-layer chromatography (TLC) until completion.[7]

At the end of the reaction, a light grey colored solid was separated out. The solid product was collected by filtration, washed several times using MeOH to eliminate impurities, and dried in an oven. The synthesized dipodal receptor 4 was then characterized using ^{1}H NMR and FT-IR spectroscopy.

Organic nanoparticles (ONPs) of receptor 4 were synthesized using the reprecipitation technique. Various quantities of the receptor (0.5 mg, 1.0 mg, 1.5 mg, and 2.0 mg) were digested in 1 mL of dimethyl sulfoxide. Under ultrasonic agitation, the solutions were progressively added to 99 mL of deionized water. This process facilitated the formation of ONPs at final concentrations of: 5 ppm, 10 ppm, 15 ppm, and 20 ppm (Scheme 1).[32]

These ONPs were subsequently used for corrosion inhibition studies in acidic media.

2.2. Preparation of corrosive media and steel coupons

Analytical reagent (AR) grade concentrated H_2SO_4 (Loba Chemie) was used to prepare 1 M sulfuric acid (H_2SO_4) solution using double distilled water. The organic nanoparticles (ONPs) of dipodal receptor 4 were then dispersed in this acidic medium to prepare test solutions at the different concentrations. The mild steel used in this study had the following composition: Fe (99.2%), Si (0.125%), C (0.105%), Mn (0.378%), S (0.079%), and P (0.0795%). Steel coupons with dimensions

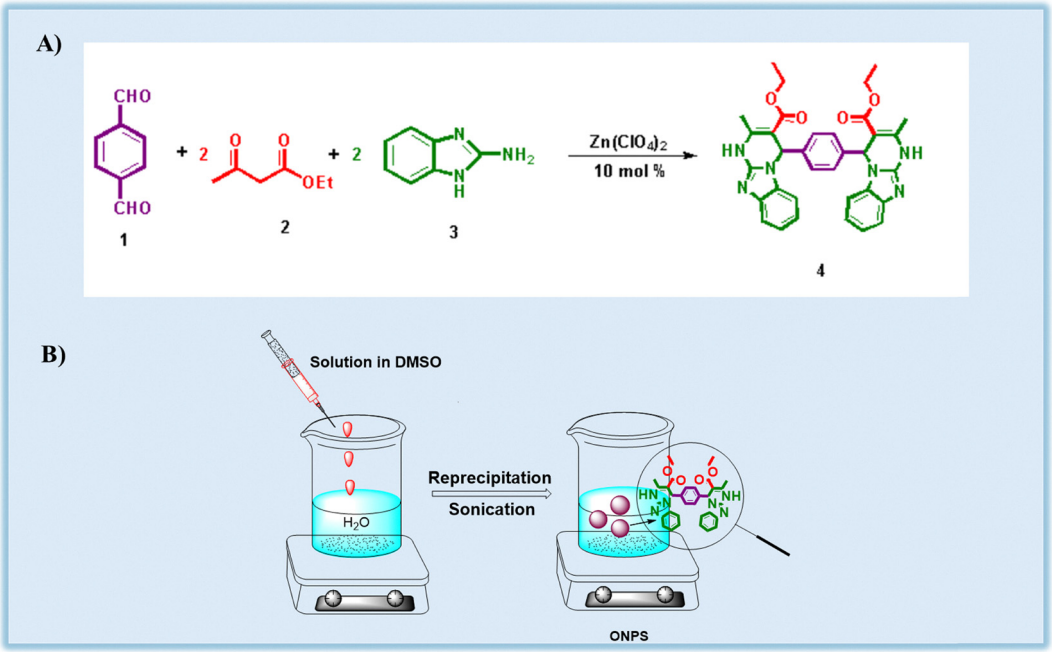

Scheme 1 (A) Preparation of dipodal receptor 4; (B) fabrication of ONPs of dipodal receptor 4.

of 1 cm × 1 cm were prepared for both gravimetric and electrochemical measurements, ensuring a consistent exposed surface area of 1 cm^2 to maintain accuracy and comparability across different methods. Prior to use, the steel coupons were mechanically polished using successive grades of emery paper (200, 400, 500, 800, and 1000 grit) to obtain a smooth and uniform surface. After polishing, the steel coupons were thoroughly cleaned with distilled water, degreased with acetone, and dried before immersion in the corrosive medium.

2.3. Gravimetric analysis

Weight loss measurements were performed in accordance with ASTM G1-03 and G31-21 standards, which outline protocols for specimen preparation, exposure, and assessment in corrosive media. Mild steel coupons were immersed in 100 mL of 1 M H_2SO_4, with and without the presence of the inhibitor, and kept at ambient temperature (25 ± 1 °C) for 24 hours. The ONPs of dipodal receptor 4 were tested at concentrations of 5, 10, 15, and 20 mg L^{-1}. Additional trials at 25 mg L^{-1} were also conducted; however, no notable increase in inhibition efficiency was observed beyond 20 mg L^{-1}. Therefore, 20 mg L^{-1} was selected as the optimum concentration for subsequent experiments. Each experiment was executed three times to ensure the reliability and reproducibility of the results.[33]

After a 24-hour exposure period:

- The mild steel coupons were carefully taken out of the solution.
- They were rinsed thoroughly with distilled water to remove any residual acid or corrosion products.
- The cleaned samples were then dried and reweighed to determine the extent of weight loss.

The inhibition efficiency (IE%) was determined using the following formula:

$$\eta\% = \frac{W_0 - W_i}{W_0} \times 100 \quad (1)$$

where W_0 is the weight loss of mild steel in blank (uninhibited) solution, and W_i is the weight loss in the presence of inhibitor. The corrosion rate was evaluated using the following formula:

$$\mathrm{CR} = \frac{\Delta W}{D \times A \times T} \times 87.6 \quad (2)$$

where CR is the corrosion rate (mm $year^{-1}$), ΔW is the weight loss of the metal specimen (g), D is the density of the steel coupon (g cm^{-3}), A is the surface area of the steel coupon (cm^2), and T is the immersion time (hours).

The factor 87.6 is a unit conversion constant that adjusts the units to express corrosion rate in millimeters per year (mm $year^{-1}$).

The surface coverage (θ), which indicates the fraction of the metal surface protected by the inhibitor, was calculated using the following expression:

$$\theta = \frac{W_0 - W_i}{W_0} \quad (3)$$

where θ is the surface coverage.

2.4. Electrochemical studies

Electrochemical studies were carried out using a Metrohm Autolab PGSTAT-204 system to investigate the corrosion performance of mild steel in 1 M sulphuric acid both without and with the addition of dipodal receptor 4-based ONPs. A conventional three-electrode setup was utilized, comprising:

• A mild steel sample as the working electrode (with an exposed surface area of 1 cm^2),

• A saturated calomel electrode (SCE) serving as the reference electrode, and

• A platinum wire functioning as the counter electrode.

To expose a fixed surface area, the steel electrode was embedded in araldite resin, leaving 1 cm^2 of surface exposed to the electrolyte. Prior to all electrochemical experiments, the system was stabilized under open circuit potential (OCP) conditions for 45 minutes to ensure equilibrium.

2.4.1. Potentiodynamic polarization (PDP). The Tafel polarization studies were carried out in the potential range of –0.1 V to +0.1 V *vs.* OCP at a scan rate of 0.001 V s^{-1}, with a current range of 100 nA to 1 mA.[31] The key parameters, such as corrosion potential (E_{corr}) and corrosion current density (i_{corr}), were extracted by extrapolating Tafel slopes from the anodic and cathodic regions. Each concentration was tested in triplicate to ensure consistency and reproducibility.

The inhibition efficiency (η%) was determined using the equation:

$$\eta\% = \frac{i_{0corr} - i_{icorr}}{i_{0corr}} \times 100 \quad (4)$$

where i_{icorr} and i_{0corr} represent the corrosion current density values with and without dipodal receptor 4, respectively.

2.4.2. Electrochemical impedance spectroscopy (EIS). EIS experiments were conducted using the same Metrohm Autolab PGSTAT-204 electrochemical workstation to further evaluate the corrosion inhibition effectiveness of the ONPs. The impedance measurements were recorded across a frequency range of 100 kHz to 0.1 Hz, with 10 data points collected per frequency decade. A sinusoidal AC perturbation of 10 mV amplitude was applied during the measurements.

The inhibition efficiency (η) was calculated using the charge transfer resistance (R_{ct}) values according to the equation:

$$\eta\% = \frac{R_p - R_p^0}{R_p} \times 100 \quad (5)$$

where R_p^0 and R_p represent the polarization resistance in the absence and presence of dipodal receptor 4 respectively.

2.5. Analysis of ultraviolet-visible spectra

The UV-visible absorption spectra of dipodal receptor 4 ONPs in 1 M sulphuric acid were recorded using a Shimadzu UV-1900 spectrophotometer. The samples were analysed in two sets:

• Solutions in which mild steel coupons were immersed for 24 hours.

• Control solutions without immersion of steel coupons.

This comparative analysis enabled the monitoring of adsorption and desorption behavior of the dipodal compound during corrosion inhibition, providing insights into the interaction mechanisms of ONPs with the mild steel surface.[33]

2.6. Quantum chemical calculations

To elucidate the inhibition mechanism of dipodal receptor 4, quantum chemical calculations were performed. Key global reactivity descriptors were computed, including:

• Highest occupied molecular orbital (E_{HOMO})
• Lowest unoccupied molecular orbital (E_{LUMO})
• Energy gap ($\Delta E = E_{LUMO} - E_{HOMO}$)
• Ionization potential (I)
• Electron affinity (A)
• Electronegativity (χ)
• Global hardness (γ)
• Number of transferred electrons (ΔN)

These parameters help in predicting the electron-donating and accepting ability of the molecule, correlating with its adsorption strength and inhibition efficiency.

The calculations were based on the following equations:[34,35]

$$\Delta E = E_{HOMO} - E_{LUMO} \quad (6)$$

$$I\ (eV) = -E_{HOMO} \quad (7)$$

$$A\ (eV) = -E_{LUMO} \quad (8)$$

$$\chi\ (eV) = -\frac{1}{2}(E_{HOMO} + E_{LUMO}) \quad (9)$$

$$\gamma\ (eV) = -\frac{1}{2}(E_{HOMO} - E_{LUMO}) \quad (10)$$

$$\Delta N = \frac{\chi_{Fe} - \chi_{inh}}{2(\gamma_{Fe} - \gamma_{inh})} \quad (11)$$

2.7. Surface inspection

Scanning electron microscopy was employed to inspect the surface structure of steel specimens before and after exposure to the corrosive environment, in the presence and absence of dipodal receptor 4. The analysis was carried out using a JEOL JSM-IT500A SEM instrument.

Three sets of specimens were examined:

• Polished and cleaned mild steel,

• Mild steel exposed to 1 M H_2SO_4 without inhibitor, and

• Mild steel exposed to 1 M H_2SO_4 containing the optimal concentration (20 ppm) of dipodal receptor 4 ONPs.

The SEM micrographs provided a comparative visual assessment of surface degradation and corrosion product formation.

3. Results and discussion

3.1. Characterisation of dipodal receptor 4

The dipodal receptor 4 was successfully synthesized using dipodal receptor 4 multicomponent reaction and isolated as a white solid in 94% yield, with a melting point of 300–303 °C. The structural characterization of the synthesized compound was carried out using ^{1}H NMR and FT-IR spectroscopy, confirming the formation of the target product (Fig. 1A and B).

^{1}H NMR (400 MHz, DMSO-D_6): δ = 10.73 (s, 2H), 7.77 (d, J = 7.8 Hz, 1H, Ar-H), 7.54 (s, 1H, Ar-H), 7.21 (s, 4H, Ar-H),

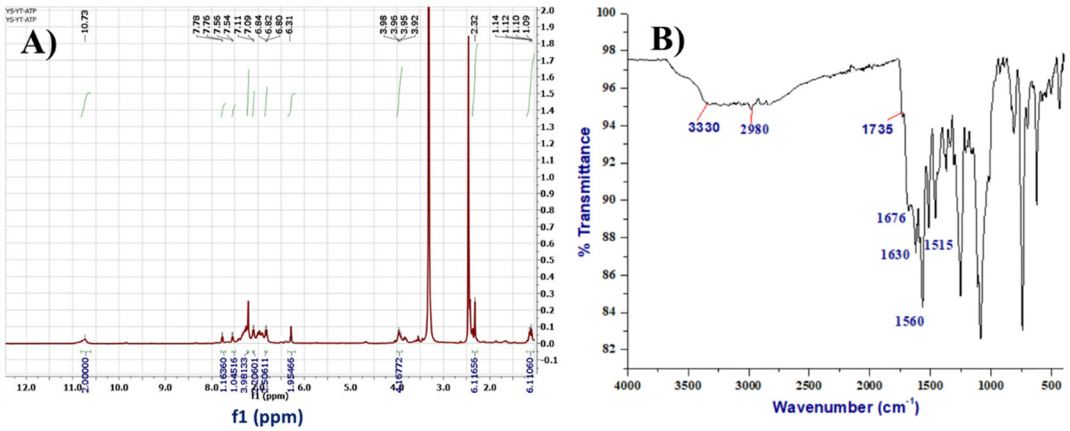

Fig. 1 (A) ^{1}H NMR spectrum of dipodal receptor 4; (B) FT-IR spectrum of dipodal receptor 4.

7.10 (d, J = 7.9 Hz, 2H, Ar-H), 6.83 (d, J = 7.7 Hz, 2H, Ar-H), 6.29 (s, 2H, CH), 3.95 (dd, J = 15.7, 9.4 Hz, 4H), 2.32 (s, 6H,), 1.11 (dd, J = 15.1, 7.8 Hz, 6H).

FT-IR (cm^{-1}): 3330 (N–H stretching), 2980 (aliphatic C–H stretching), 1735 (ester C═O), 1676 (amide C═O, amide I), 1630 (C═N stretching/conjugated C═C), and 1560–1515 (aromatic C═C stretching and amide II band).

These spectral results confirm the successful formation of dipodal receptor 4 with key functional groups consistent with the proposed structure.

3.2. Gravimetric analysis

Gravimetric studies were carried out to assess the corrosion inhibition performance of dipodal receptor 4 ONPs in 1 M H_2SO_4 at varying concentrations ranging from 5 to 20 mg L^{-1}. The experimental findings are presented in Table 1. Surface coverage (θ) and inhibition efficiency (η%) were calculated using eqn (1), based on the variation in mass loss of mild steel specimens in the absence and presence of the inhibitor.

The results reveal a clear trend: as the concentration of ONPs increases, the corrosion rate consistently decreases. This behavior is attributed to stronger adsorption of the nanoparticles onto the steel surface, which is likely facilitated by the presence of heteroatoms and π-electron-rich regions in the receptor structure. These interactions promote the creation of a defensive layer that shields the metal from proton-induced degradation in the acidic environment.[33]

At 5 mg L^{-1}, the inhibition efficiency was observed to be 57.10%, which increased to 75.18% at 15 mg L^{-1} and reached a peak of 90.14% at 20 mg L^{-1}. The minimal improvement beyond 20 mg L^{-1} indicates that the steel surface becomes saturated with inhibitor molecules, designating 20 mg L^{-1} as the optimal concentration for effective corrosion resistance under these conditions.

3.3. Characterisation of dipodal receptor 4 ONPs

As dipodal receptor 4 ONPs displayed maximum inhibition efficiency at 20 mg L^{-1}, the hydrodynamic radius of the ONPs at this concentration was examined. The dynamic light scattering (DLS) histogram revealed that the average particle size of 4 ONPs at this concentration is 32 nm (Fig. 2A). Furthermore, zeta potential analysis was performed using a zeta check particle charge reader. The ONPs of dipodal receptor 4 (20 mg L^{-1}) showed a zeta potential of −15 mV, which indicates the stability of ONPs. On changing the pH of the medium toward more basic and more acidic, significant variation in the zeta potential was observed. This can be attributed to the hydrolysis of ester functional groups on the surface of the ONPs. In basic media, the ONPs showed a zeta potential of −34 mV whereas in acidic media the observed value of zeta potential was −24 mV (Fig. 2B).

3.4. Langmuir adsorption isotherm

Adsorption isotherms describe the relationship between the surface of steel and corrosion inhibitor molecules.[30] Steel surfaces are coated with corrosion inhibitors, which reduce corrosion rates. The dipodal receptor 4 adsorption on the steel surface increases with increasing ONP concentration on the surface. Fig. 3 illustrates the graph between C/θ and C with a linear relationship with R^2 0.99. A high R^2 value, such as 0.98,

Table 1 Calculated inhibition efficiency and surface coverage of OPNs of dipodal receptor 4

Medium used	Dipodal receptor 4 concentration (mg L^{-1})	Weight loss (g ms) (ΔW)	Surface coverage (θ) by dipodal receptor 4	Inhibition efficiency (η%)
1 M H_2SO_4	Blank (0)	2.94	—	—
	5	1.26	0.5710	57.10
	10	1.02	0.6519	65.19
	15	0.73	0.7518	75.18
	20	0.29	0.9014	90.14

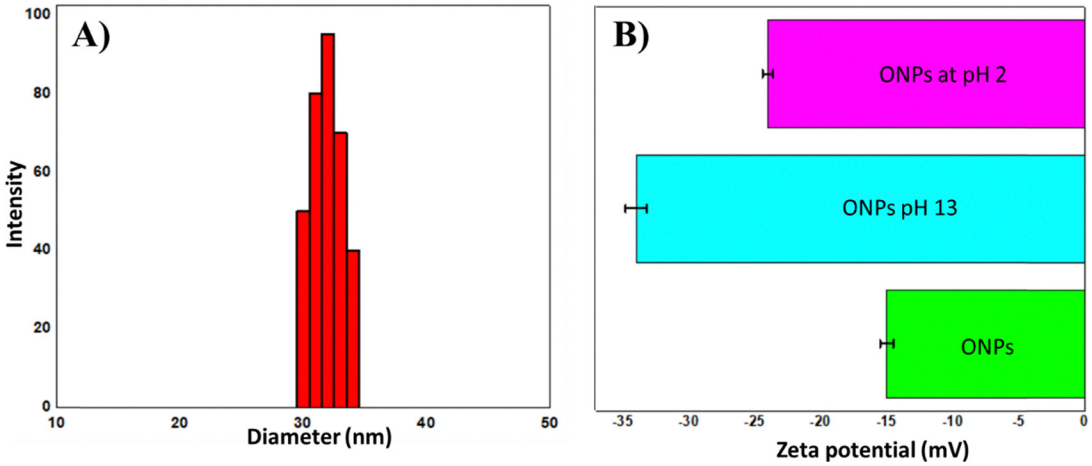

Fig. 2 (A) DLS micrograph for OPNs of dipodal receptor 4; (B) zeta potential analysis of ONPs of dipodal receptor 4.

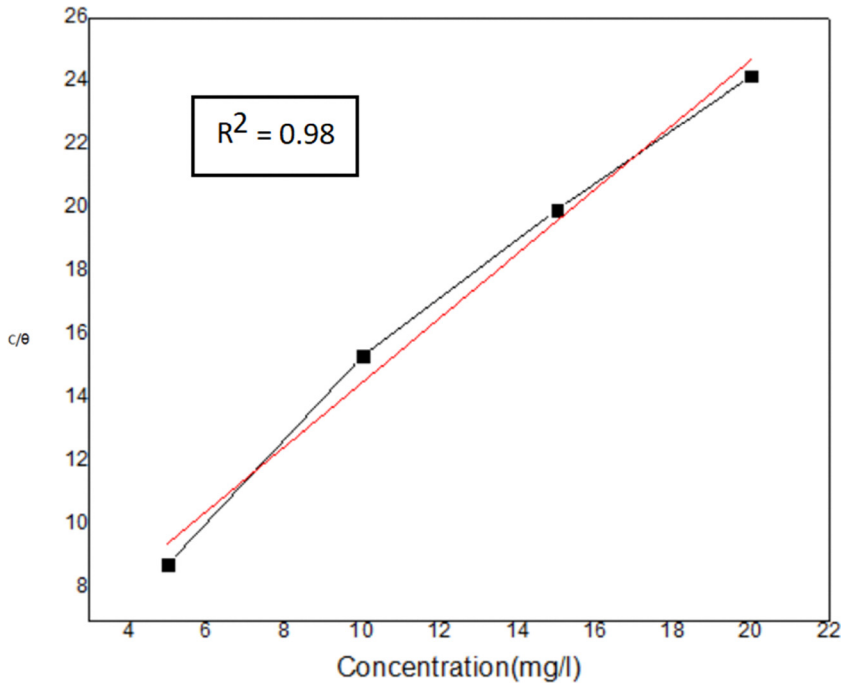

Fig. 3 The Langmuir adsorption isotherm at different concentrations of dipodal receptor 4 ONPs in 1 M sulphuric acid for steel.

indicates a strong linear correlation between the variables, suggesting that the model accurately represents the relationship between derivative concentration and adsorption on the steel surface. This strong fit implies that as the concentration of the dipodal receptor 4 increases, its adsorption on the steel surface increases in a predictable manner, effectively reducing corrosion. The value of K_{ads} calculated by using eqn (12) is 0.458. The K_{ads} value was used to calculate the ΔG value by eqn (13).

Eqn (12) describes the relationship between the adsorption of dipodal receptor 4 on the surface of steel

$$\frac{C}{\theta} = \frac{1}{K_{ads}} + C \qquad (12)$$

where θ is the surface coverage, C is the concentration of the inhibitor (mg L^{-1}), and K_{ads} is the adsorption equilibrium constant.

The linear relationship indicates that the adsorption process follows the Langmuir model, suggesting monolayer adsorption on a homogeneous metal surface.

The standard free energy of adsorption (ΔG^0_{ads}) is calculated using the following thermodynamic equation:

$$\Delta G^0_{ads} = -RT\ln(55.5 \times K_{ads}) \qquad (13)$$

where R is the representation of the gas constant, T indicates the absolute temperature, ΔG^0_{ads} is the standard free energy of

adsorption and C_{water} is the concentration of H_2O in the solution. According to thermodynamic criteria:

• If $\Delta G^0_{ads} > -20$ kJ mol^{-1}, the adsorption process is considered physical adsorption (physisorption), involving weak van der Waals or electrostatic interactions.

• If $\Delta G^0_{ads} < -40$ kJ mol^{-1}, the process is attributed to chemical adsorption (chemisorption), involving charge sharing or transfer (coordinate bonding) between inhibitor molecules and the metal surface.

In this case, the ΔG^0_{ads} value of -8.0 kJ mol^{-1} suggests that dipodal receptor 4 is physically adsorbed on the steel surface, predominantly *via* electrostatic interactions. Although the adsorption is relatively weak, effective corrosion mitigation can be achieved through the surface coverage under acidic conditions, especially at higher inhibitor concentration. It should be noted that the present electrochemical measurements reflect short-term inhibition efficiency. Further long-term immersion and stability study would be essential to evaluate corrosion protection under extended exposure conditions.

3.5. Electrochemical investigations

3.5.1. Potentiodynamic polarization (PDP) study. Dipodal receptor 4 demonstrates considerable effectiveness as a corrosion inhibitor by mitigating both anodic and cathodic processes involved in the corrosion of mild steel. Its inhibitory performance was assessed through Tafel polarization, focusing on changes in corrosion current density (i_{corr}).

As shown in Fig. 4A, the introduction of dipodal receptor 4 leads to a noticeable shift in the polarization curves toward lower i_{corr} values, indicating a reduced rate of electrochemical reactions. This behavior reflects a suppression of both metal dissolution and hydrogen release reactions, thereby improving the corrosion resistance of mild steel in acidic conditions. Table 2 provides the corresponding electrochemical parameters, including anodic and cathodic Tafel slopes (β_a and β_c), corrosion potential (E_{corr}), and calculated inhibition efficiencies.

The marked decline in i_{corr} affirms the strong inhibitory effect of receptor 4, which is attributed to its adsorption onto the metal surface, forming a protective layer that limits electron transfer. Minor variations in β_a and β_c values across different concentrations suggest that the compound influences both anodic and cathodic reactions. This dual action, along with E_{corr} shifts of less than $\pm$85 mV, confirms the behavior of dipodal receptor 4 as a mixed-type inhibitor. The parallel nature of the Tafel lines before and after inhibitor addition implies that the mechanism of corrosion remains unchanged, and the inhibitor primarily reduces the rate of the process rather than altering the pathway. Moreover, the inhibition efficiency was found to increase with inhibitor concentration, confirming concentration-dependent protection. Various concentrations of dipodal receptor 4 demonstrated its ability to interfere with multiple electrochemical processes, including iron oxidation at the anode and hydrogen evolution at the cathode.

At a concentration of 20 mg L^{-1}, dipodal receptor 4 exhibited the highest inhibition efficiency of 91.36%, corresponding to a minimum corrosion current density of 1.9×10^{-5} A cm^{-2}. These findings, summarized in Table 2, confirm that the corrosion inhibition performance is directly related to the compound's adsorption ability, which effectively reduces the exposed area of the metal and thereby minimizes corrosion.

3.5.2. Electrochemical impedance spectroscopy. Fig. 4(B) and (C) display the Nyquist and Bode plots, respectively, while Fig. 4(E) shows the equivalent electrical circuit used to fit the data. Before the electrochemical study (EIS), the working electrode was immersed in the test solution to set the OCP. The OCP was allowed to stabilize for 45 minutes until a quasi-steady state was achieved. The OCP *vs.* time curve presented in Fig. 4(F) confirmed the stabilization before performing EIS and polarization measurements. The corresponding numerical values are summarized in Table 3. The size of the capacitive semicircles in the Nyquist plots reflects the corrosion protection ability of dipodal receptor 4. As the concentration of the inhibitor increased in the 1 M H_2SO_4 solution, the diameter of these semicircles also grew, indicating a significant reduction in mild steel dissolution. This increase in charge transfer resistance (R_{ct}), as seen in Table 3, points to enhanced inhibition efficiency. The improved R_{ct} values suggest that dipodal receptor 4 forms an adsorbed protective film on the steel surface, which hinders the movement of charges and limits the penetration of aggressive ions from the acidic solution.

The double-layer capacitance (C_{dl}) was calculated using the equation:

$$C_{dl} = (QR_{ct}^{1-n})^{1/n} \quad (14)$$

The Bode phase angle plots reveal a noticeable shift toward lower frequencies following the addition of dipodal receptor 4, indicating enhanced surface coverage and improved barrier formation. The Bode impedance plots (Fig. 4C) further support this trend. The absolute impedance values ($|Z|$) at lower frequencies increase significantly with increasing inhibitor concentration, which directly demonstrates an increase in polarisation resistance and improved corrosion protection. As the low frequency impedance modulus is directly proportional to the overall resistance of the metal and electrolyte interface. The high values of $|Z|$ on addition of dipodal receptor 4 indicate the suppression of charge transfer processes. At 20 mg L^{-1}, the highest value of $|Z|$ demonstrates the formation of a highly resistive and stable protective layer. In the intermediate frequency region, the slope of $\log|Z|$ *versus* $\log f$ approaches -1, which depicts the dominant capacitive behaviour and confirms that the corrosion process remains charge transfer controlled.

The Bode phase angle (θ) plots provide significant insight into surface characteristics. In the uninhibited solution, the maximum phase angle is relatively lower and broader, which indicates the surface heterogeneity and active dissolution sites. On addition of the inhibitor (receptor 4), the maximum phase angle increases and shifts towards lower frequency values demonstrating the improved surface homogeneity and formation of a thicker adsorbed film with longer relaxation time constants. The broader and higher phase angle peak signifies

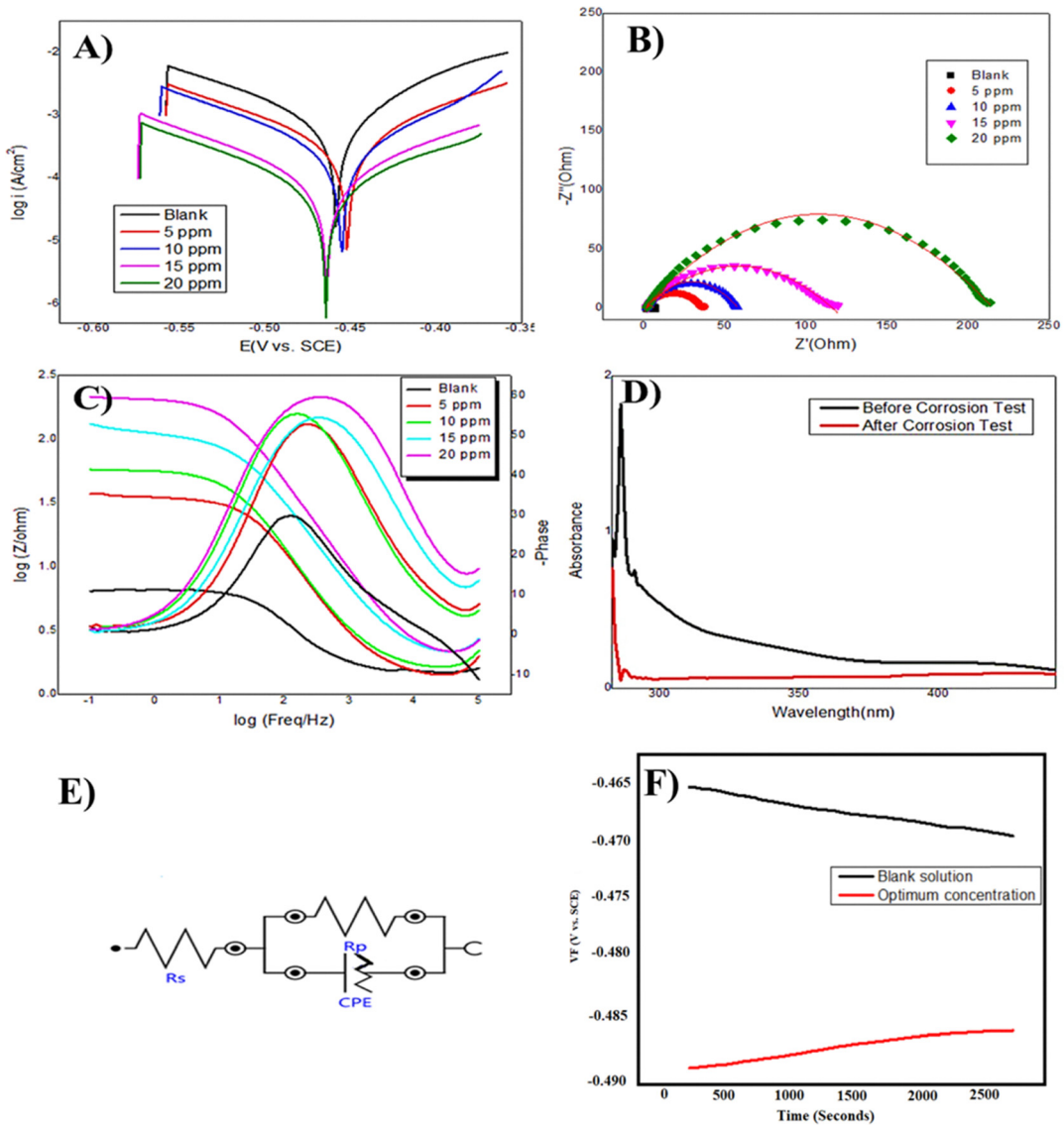

Fig. 4 (A) Tafel polarization curves of mild steel in 1 M H_2SO_4 in the absence and presence of various concentrations of dipodal receptor 4, showing the shift in current density and corrosion potential; (B) Nyquist plots for mild steel in 1 M H_2SO_4 without and with different concentrations of dipodal receptor 4 at 298 K, illustrating changes in charge transfer resistance; (C) Bode plots for mild steel in 1 M sulphuric acid without and with dipodal receptor 4 at 298 K, highlighting impedance behavior across frequencies; (D) UV-Vis spectra of the dipodal receptor 4 solution before and after immersion of steel specimens, showing molecular interaction and potential adsorption during corrosion inhibition. (E) Electrochemical circuit fit. (F) Open circuit potential (OCP) graph.

Table 2 Polarization parameters in 1 M sulphuric acid with and without various concentrations of ONPs of dipodal receptor 4

Dipodal receptor 4 concentration (mg L^{-1})	β_c (V dec^{-1})	β_a (V dec^{-1})	E_{corr} (V *versus* SCE)	Corrosion rate (mm $year^{-1}$)	i_{corr} (A cm^{-2})	Inhibition efficiency
0	0.06263	0.09527	−0.506	34.03	2.2×10^{-4}	0
5	0.095	0.103	−0.452	3.297	1.3×10^{-4}	40.90
10	0.090	0.095	−0.464	2.452	5.9×10^{-5}	73.18
15	0.095	0.095	−0.464	0.947	3.4×10^{-5}	84.54
20	0.087	0.075	−0.455	0.691	1.9×10^{-5}	91.36

enhanced capacitive behaviour and better barrier properties. These observations are in good agreement with the equivalent circuit model (Fig. 4E), where charge transfer resistance is in parallel with the constant phase element (CPE), indicating non-ideal capacitive behaviour due to surface roughness. This observation, combined with the observed increase in polarization resistance (R_p), provides strong evidence for the effective adsorption of the inhibitor onto the mild steel surface. At an

Table 3 EIS parameters for steel in 1 sulphuric acid at different concentrations of dipodal receptor 4

Corrosive media	Concentration compound (mg L^{-1})	R_s (Ω cm^2)	CPE (μF cm^{-2})	R_{ct} (Ω cm^2)	N	Inhibition efficiency (%)
1 M H_2SO_4	Blank (0)	1.48	5.2×10^{-4}	5.22	0.83	—
	5	1.59	12×10^{-5}	33.77	0.82	84.54
	10	1.87	14×10^{-5}	55.43	0.82	90.58
	15	1.93	5.73×10^{-5}	114.45	0.80	95.43
	20	2.52	4.5×10^{-5}	208.91	0.80	97.50

optimal concentration of 20 mg L^{-1}, the receptor exhibited a peak inhibition efficiency of 97.50%, demonstrating outstanding corrosion protection capability.

Despite the variation in inhibitor concentration, the impedance spectra showed only minor differences in shape, suggesting that the fundamental corrosion mechanism at the metal–electrolyte interface remained unchanged.[36] One of the key parameters used to evaluate inhibitor performance is the double-layer capacitance C_{dl}. A decline in C_{dl} generally indicates that the inhibitor is reinforcing the protective film on the metal surface. This decrease is attributed to a reduction in the local dielectric constant and an increase in the thickness of the electrical double layer, resulting from inhibitor adsorption.[37]

As presented in Table 3, the C_{dl} values for the systems containing dipodal receptor 4 are significantly lower than those of the uninhibited solution. This confirms the formation of a compact inhibitor layer on the metal surface, effectively minimizing exposure to the acidic medium and enhancing the corrosion resistance of mild steel.

In the absence of an inhibitor, a smaller phase angle (which indicates restrictive capacitive behavior) results in lower impedance at low frequencies, as demonstrated by the Bode plot. Following the addition of the corrosion inhibitor, there is a notable increase in low-frequency impedance and an increase in phase angles at both low and mid frequencies, which signifies an enhancement in the corrosion resistance of the solution.[35]

3.6. Ultraviolet-visible spectra

The UV-vis spectra of dipodal receptor 4 were recorded both before and after exposure to corrosive conditions to understand its interaction with the metal surface. As shown in Fig. 4D, distinct differences in absorbance levels were observed between two systems: one containing dipodal receptor 4 in acidic media alone, and the other with mild steel immersed in the same media for 24 hours.

These differences—particularly in peak intensity and wavelength shifts—suggest that dipodal receptor 4 interacts with both the acidic environment and corrosion products, likely coordinating with Fe^{2+} and Fe^{3+} ions released from the steel surface. The spectral changes indicate that the compound remains stable in acidic conditions and has a strong tendency to adsorb onto the metal surface. This adsorption process is crucial to forming a protective barrier that helps mitigate corrosion. In effect, the dipodal receptor not only resists degradation in harsh media but also establishes a complex with the metal ions, forming a stable, protective layer over the steel.

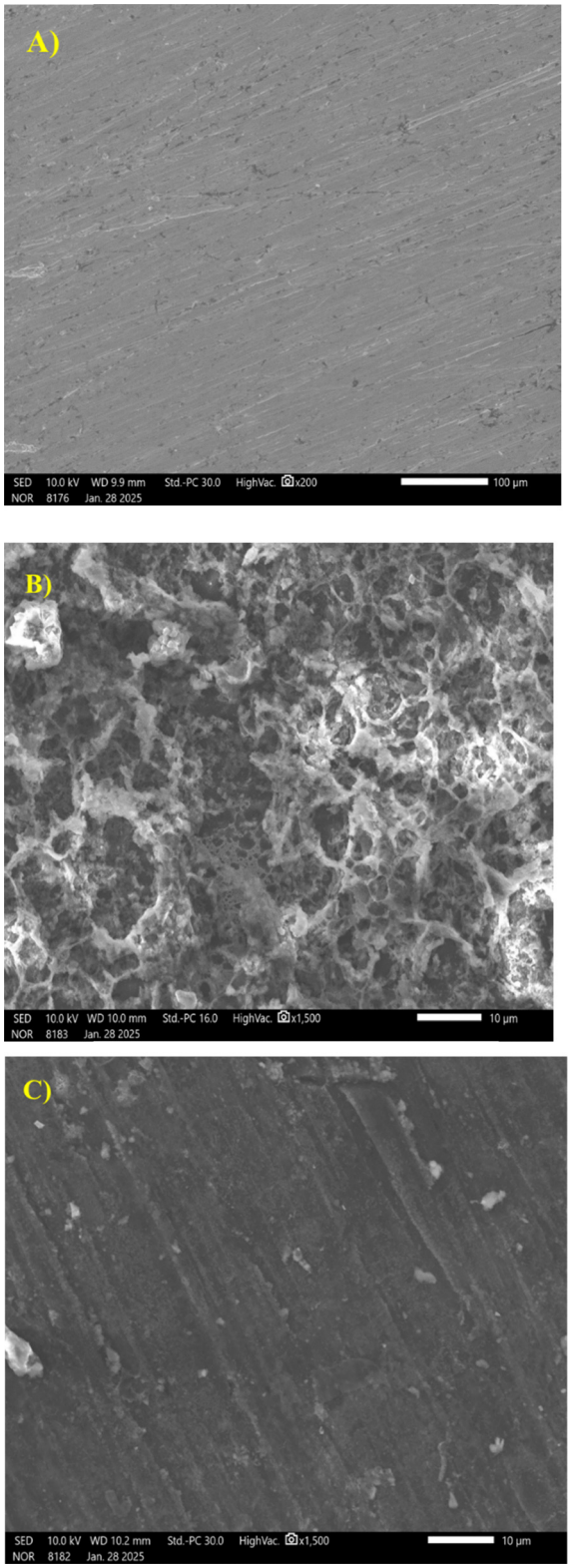

Fig. 5 Surface morphology of cleaned steel (A), corroded steel immersed in 1 M H_2SO_4 (B) and the inhibited surface (C).

3.7. Surface inspection by scanning electron microscopy

To investigate the surface conditions of mild steel after corrosion testing, SEM analysis was performed by utilizing a low-energy electron beam at 10 kV to avoid damaging the inhibitor layer. This analysis compared the surface morphologies of steel samples before and after 24 hour immersion in 1 M sulphuric acid, with and without the addition of 20 mg L^{-1} of dipodal receptor 4.[38]

As shown in Fig. 5A, the untreated steel surface was smooth and free from any visible corrosion. In contrast, the sample immersed in acid without the inhibitor (Fig. 5B) exhibited significant surface degradation, marked by roughness and pitting due to aggressive corrosion. However, the sample treated with dipodal receptor 4 (Fig. 5C) showed notably less damage. The surface remained relatively intact, suggesting that the dipodal receptor 4 formed a protective film that effectively minimized acid-induced corrosion.

These observations confirm the dipodal receptor's ability to act as a surface-active compound, reducing corrosion through film formation and metal–ligand interaction.

3.8. Quantum chemical calculations

To gain deeper insights into the inhibition mechanism of dipodal receptor 4, quantum chemical calculations were conducted. The optimized geometry of the receptor is presented in Fig. 6A, while the highest occupied molecular orbital (HOMO) and the lowest unoccupied molecular orbital (LUMO) are depicted in Fig. 6B and C, respectively. The analysis of frontier molecular orbitals is essential for assessing the molecule's electron transfer characteristics during its interaction with the metal surface. The HOMO is associated with the molecule's capacity to donate electrons to the metal, facilitating adsorption through donor–acceptor interactions. Conversely, the LUMO reflects the ability of the molecule to accept electrons from the metal surface. The energy gap (ΔE) between the HOMO and LUMO is a crucial indicator of chemical reactivity—smaller ΔE values generally suggest higher reactivity and stronger adsorption potential, both of which are desirable for effective corrosion inhibition. As shown in Table 4, a smaller ΔE value correlates with greater inhibition efficiency. This suggests that dipodal receptor 4, having a lower ΔE, can easily interact with the metal surface to form a stable, protective layer, thus reducing the rate of corrosion. Additionally, a higher electronegativity (χ) and greater electron-donating ability (as indicated by the calculated ΔN values) further support the compound's strong adsorption behavior and effective corrosion protection. These theoretical insights reinforce the experimental findings, confirming dipodal receptor 4 as an efficient corrosion inhibitor through its favourable electronic properties and strong interaction with the metal surface.[39–43]

Table 4 Theoretical parameters for dipodal receptor 4

Parameters (eV)	Value for dipodal receptor 4 (eV)
E_{HOMO}	−0.24275
E_{LUMO}	−0.24165
ΔE	0.0011
I	0.24275
A	0.24165
χ	0.2422
γ	0.00055

3.9. Proposed corrosion inhibition mechanism of dipodal receptor 4 on mild steel in 1 M sulphuric acid

The excellent corrosion inhibition efficiency of dipodal receptor 4 is closely linked to its molecular architecture, which features multiple electron-donating functional groups such as carbonyl, amino, and hydroxyl moieties, along with aromatic rings. These groups possess lone pairs of electrons that can coordinate with the metal surface, promoting strong adsorption through donor–acceptor interactions. Such adsorption behavior significantly contributes to mitigating corrosion in 1 M sulfuric acid.[44]

Once adsorbed, dipodal receptor 4 establishes a compact and adherent protective film over the mild steel surface, as illustrated in Fig. 7A. This film serves as both a physical shield and a chemical barrier, impeding the electrochemical reactions responsible for corrosion. The presence of π-electron systems and heteroatoms with available lone pairs enhances the receptor's ability to form stable coordination bonds with the vacant d-orbitals of surface iron atoms. This strengthens the inhibitor–metal interaction and amplifies the overall inhibition performance.

To understand the mechanism more clearly, it is important to consider the electrochemical environment. In 1 M H_2SO_4,

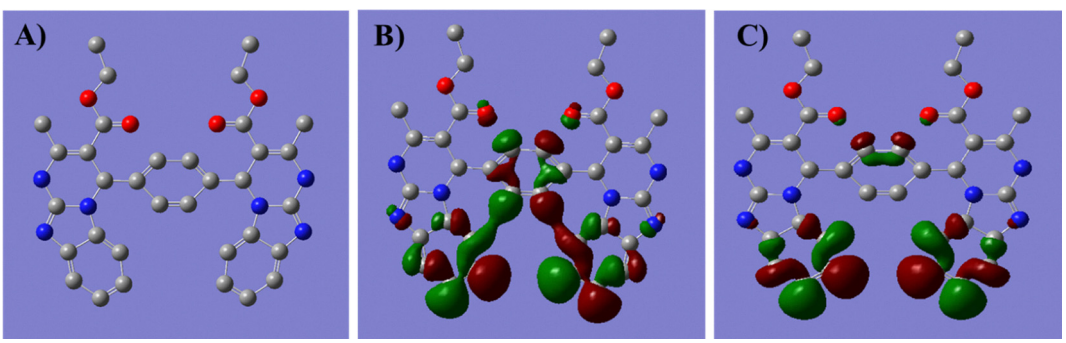

Fig. 6 (A) Optimized structure of dipodal receptor 4, (B) HOMO of dipodal receptor 4, and (C) LUMO of dipodal receptor 4.

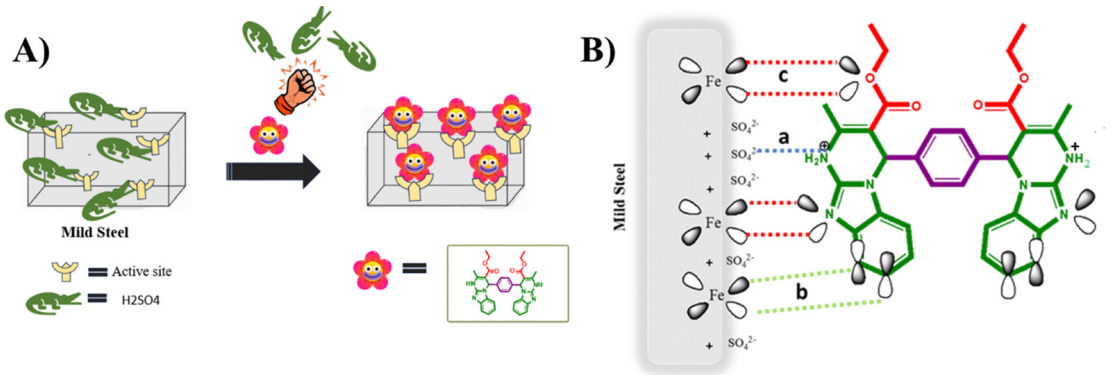

Fig. 7 (A) Artistic representation of corrosion inhibition of steel by dipodal receptor 4, and (B) schematic representation of adsorption of dipodal receptor 4 on steel in 1 M H_2SO_4.

mild steel surfaces tend to acquire a positive charge relative to the potential of zero charge (PZC), while dipodal receptor 4 can exist either in a neutral or protonated (cationic) form. This allows for multiple modes of interaction at the metal/solution interface (Fig. 7B), including:

- Electrostatic interaction between protonated inhibitor molecules and pre-adsorbed sulphate anions on the steel surface (represented by a).
- π-electron interactions between the aromatic rings of the receptor and vacant d-orbitals of iron atoms (represented by b).
- Coordinate bonding between lone pairs on heteroatoms (*e.g.*, N, O) and the metal surface (represented by c).

These combined interactions contribute to the creation of a stable inhibitor covering that shields the metal from aggressive ions in the acidic medium.

Furthermore, the corrosion inhibition property of dipodal receptor 4 was compared with other heterocyclic pyrimidinone-based derivatives (Table 5). The results show that the synthesized dipodal receptor exhibits superior inhibition efficiency even at low concentrations. This is likely due to the presence of two pyrimidinone moieties within its structure, enhancing its ability to cover more surface area and anchor more effectively to the steel substrate.

The efficiency of dipodal receptor 4 was also compared with other heterocyclic derivatives containing pyrimidinone units, as outlined in Table 5. To ensure methodological consistency, the inhibition efficiency given in Table 5 is derived from electrochemical techniques such as PDP and EIS. The highest inhibition efficiency values reported from the EIS and PDP measurements are presented for comparative purposes. It is very important to note the variation in electrolyte composition; in particular, the presence of an aggressive medium like chloride ions and sulphate ions can significantly influence the corrosion mechanism and inhibitor adsorption behaviour. Therefore, electrochemical measurements may remain consistent, and differences in corrosive medium may affect the inhibition performance. The results clearly demonstrate that receptor 4 exhibits superior inhibitory performance, even at relatively low concentrations. This improved efficiency is likely due to the presence of two pyrimidinone moieties within its

Table 5 Comparison of dipodal receptor 4 as a corrosion inhibitor with other reported inhibitors for steel in HCl and H_2SO_4 media

S. no.	Derivative	Conc. (ppm)	Media	Efficiency (%)	Technique	Ref.
1	1,2,3-Triazole derivative of dihydropyrimidinones	10	1 M HCl	95	EIS	20
2	Pyrimidinone-linked thiazoles	100	1 M HCl	69.35	PDP	34
3	Ethyl 4-[4-(dimethylamino)phenyl]-2-imino-6-methyl-1,2,3,4-tetrahydropyrimidine-5-carboxylate (EDTP)	750	1 M HCl	87.6	EIS	35
4	Tetrahydropyridines	40	1 M HCl	90.67	PDP	36
5	5-Acetyl-4-[4-(dimethylamino)phenyl]-6-methyl-3,4-dihydropyrimidin-2(1*H*)-one (ADP)	750	1 M HCl	88.9	PDP	37
6	Quinolone derivative, namely, (*E*)-2-amino-7-hydroxy-4-styrylquinoline3-carbonitrile	100	3.5% NaCl	89	PDP	38
7	Schiff base from melamine and isatin	17.5	0.5 M HCl	91.60	EIS	39
8	8-(4-Methoxyphenyl)-3,6-dioxo-2-(*p*-tolyl)-3,6-dihydro-2*H*-thiazolo[3′,2′:2,3][1,2,4]triazolo[1,5-*a*]pyrimidine-7-carbonitrile	588	1 M HCl	87.8	PDP	44
9	Fmoc centered peptide conjugate	400	1 M HCl	72.2	EIS	45
10	Pyran chloro derivatives	344	1 M HCl	88.8	EIS	46
11	Nicotinic acid–amino acid derivatives	200	1 M HCl	81.23	PDP	47
12	Spiro-pyrazoline-butyrolactone	382	1 M HCl	86.17	EIS	48
12	2-(3-Nitrophenyl)imidazo[1,2-*a*]pyridine	239	1 M HCl	91.47	PDP	49
13	Dipodal receptor 4	20	1 M H_2SO_4	97.50	EIS	This work

molecular framework, which enhances its surface coverage and facilitates stronger adsorption on the steel surface.

The presence of dual coordination canters enables the receptor to form a more cohesive and stable protective film across the metal interface. This contributes to its ability to effectively block both anodic and cathodic corrosion reactions, resulting in enhanced corrosion resistance compared to other structurally related compounds.

4. Conclusion

Corrosion inhibition efficiency is markedly improved by application of dipodal receptor 4, achieving a maximum of 97.50% at a concentration of 20 mg L^{-1}, as evidenced by electrochemical impedance spectroscopy (EIS). This superior performance is attributed to the molecular architecture of the receptor, which features multiple electron-rich centers that promote robust adsorption onto the mild steel surface. Electrochemical analyses confirmed a direct correlation between inhibitor concentration and corrosion protection efficiency. Moreover, surface morphology studies revealed the formation of a uniform and adherent protective film that effectively isolates the metal from acidic environments, thereby minimizing degradation. Although density functional theory (DFT) calculations provide valuable insight into the electronic characteristics and adsorption propensity of the inhibitor, further validation using adsorption isotherm models such as the Langmuir isotherm and thermodynamic parameters like (ΔG^0_{ads}) would offer a more comprehensive understanding of the inhibitor's adsorption mechanism on mild steel.

Author contributions

Amisha Yadav: conceptualization, data curation, and methodology; Jasdeep Kaur: validation, editing, and writing – original draft preparation; Amanpreet Singh: visualization, investigation, and supervision; Ankush Kumar Tangra: methodology and validation; Gurjaspreet Singh: investigation and visualization.

Conflicts of interest

The authors declare that they have no known competing financial interests or personal relationships that could have appeared to influence the work reported in this paper.

Data availability

Data will be made available upon request.

References

1 M. McGuinness and D. Dowling, Plant-associated bacterial degradation of toxic organic compounds in soil, *Int. J. Environ. Res. Public Health*, 2009, **6**(8), 2226–2247.
2 N. Nirwan, C. Pareek and A. Chohadia, Role of Nitrogen-containing natural heterocyclic compounds in medical science: A Mini Review, *IJSRST*, 2015, **1**(1), 76–84.
3 A. Amin, T. Qadir, P. K. Sharma, I. Jeelani and H. Abe, A review on the medicinal and industrial applications of N-containing heterocycles, *Open Med. Chem. J.*, 2022, **16**(1), e187410452209010.
4 P. Arora, V. Arora, H. S. Lamba and D. Wadhwa, Importance of heterocyclic chemistry: a review, *Int. J. Pharm. Sci. Res.*, 2012, **3**(9), 2947.
5 E. Kabir and M. Uzzaman, A review on biological and medicinal impact of heterocyclic compounds, *Results Chem.*, 2022, **4**, 100606.
6 J. Sharma and R. Kaushal, Nitrogen Containing Heterocyclic Chalcone Hybrids and Their Biological Potential (A Review), *Russ. J. Gen. Chem.*, 2024, **94**(7), 1794–1814.
7 A. Singh, G. Singh, S. Sharma, N. Kaur and N. Singh, Metal-Free, Biomass-Derived Nano-Architectured Carbon Quantum Dots as an Efficient Acid-Base Bifunctional Catalyst for Facile Synthesis of Benzo[*g*]chromene and Pyrimidine Analogs, *ChemistrySelect*, 2022, **7**(29), e202200942.
8 A. Rusu, I. M. Moga, L. Uncu and G. Hancu, The role of five-membered heterocycles in the molecular structure of antibacterial drugs used in therapy, *Pharmaceutics*, 2023, **15**(11), 2554.
9 N. Jangir, Poonam, S. Dhadda and D. K. Jangid, Recent advances in the synthesis of five-and six-membered heterocycles as bioactive skeleton: a concise overview, *ChemistrySelect*, 2022, **7**(6), e202103139.
10 S. Sharma and S. Singh, The biological and pharmacological potentials of Indole-based heterocycles, *Lett. Org. Chem.*, 2023, **20**(8), 711–729.
11 S. V. Mamatha, M. Bhat, H. K. Kumara, D. C. Gowda, M. Tirukoti and S. K. Meenakshi, Design, synthesis and SAR evaluation of mercaptooxadiazole analogs as anti-tubercular, anti-diabetic and anti-bacterial agents, *Chem. Data Collect.*, 2020, **26**, 100343.
12 S. Kumari, S. K. Gupta and L. Tiwari, A Review on synthesis, Characterization, Pharmacological activity of 1,2,3 triazole derivatives containing benzothiazole, *Int. J. Pharm. Erudition*, 2021, **11**(20), 22–48.
13 Y. M. Zohny, S. M. Awad, M. A. Rabie and O. A. Al-Saidan, Synthesis of dihydropyrimidines: isosteres of nifedipine and evaluation of their calcium channel blocking efficiency, *Molecules*, 2023, **28**(2), 784.
14 A. M. Farghaly, O. M. AboulWafa, Y. A. Elshaier, W. A. Badawi, H. H. Haridy and H. A. Mubarak, Design, synthesis, and antihypertensive activity of new pyrimidine derivatives endowing new pharmacophores, *Med. Chem. Res.*, 2019, **28**, 360–379.
15 P. K. Maji, Recent progress in the synthesis of pyrimidine heterocycles: a review, *Curr. Org. Chem.*, 2020, **24**(10), 1055–1096.
16 M. Funicello, I. Cerminara, L. Chiummiento, P. Lupattelli, F. Felluga and F. Berti, Biginelli reaction and β-secretase inhibition: a multicomponent reaction as a friendly

educational approach to bioactive compounds, *J. Chem. Educ.*, 2021, **98**(5), 1756–1761.
17 R. Kaur, S. Chaudhary, K. Kumar, M. K. Gupta and R. K. Rawal, Recent synthetic and medicinal perspectives of dihydropyrimidinones: a review, *Eur. J. Med. Chem.*, 2017, **132**, 108–134.
18 F. Sánchez-Sancho, M. Escolano, D. Gaviña, A. G. Csáky, M. Sánchez-Roselló, S. Díaz-Oltra and C. Del Pozo, Synthesis of 3,4-dihydropyrimidin (thio) one containing scaffold: Biginelli-like reactions, *Pharmaceuticals*, 2022, **15**(8), 948.
19 S. Gulati, S. E. John and N. Shankaraiah, Microwave-assisted multicomponent reactions in heterocyclic chemistry and mechanistic aspects, *Beilstein J. Org. Chem.*, 2021, **17**(1), 819–865.
20 R. González-Olvera, V. Román-Rodríguez, G. E. Negrón-Silva, A. Espinoza-Vázquez, F. J. Rodríguez-Gómez and R. Santillan, Multicomponent synthesis and evaluation of new 1,2,3-triazole derivatives of dihydropyrimidinones as acidic corrosion inhibitors for steel, *Molecules*, 2016, **21**(2), 250.
21 H. A. Younus, M. Al-Rashida, A. Hameed, M. Uroos, U. Salar, S. Rana and K. M. Khan, Multicomponent reactions (MCR) in medicinal chemistry: a patent review (2010–2020), *Expert Opin. Ther. Pat.*, 2021, **31**(3), 267–289.
22 M. J. Climent, A. Corma and S. Iborra, Homogeneous and heterogeneous catalysts for multicomponent reactions, *RSC Adv.*, 2012, **2**(1), 16–58.
23 F. Sánchez-Sancho, M. Escolano, D. Gaviña, A. G. Csáky, M. Sánchez-Roselló, S. Díaz-Oltra and C. Del Pozo, Synthesis of 3,4-dihydropyrimidin (thio) one containing scaffold: Biginelli-like reactions, *Pharmaceuticals*, 2022, **15**(8), 948.
24 A. Singh and J. Kaur, Multicomponent Reactions for Eco-compatible Heterocyclic Synthesis Over Solid Base Catalysts, *Solid Base Catalysts: Synthesis, Characterization, and Applications*, 2024, pp. 153–167.
25 H. T. Rahal, A. M. Abdel-Gaber, R. Al-Oweini and R. N. El-Tabesh, Corrosion inhibition and adsorption properties of some manganese metal complexes on mild steel in sulfuric acid solutions, *Int. J. Corros. Scale Inhib.*, 2024, **13**(2), 708–726.
26 A. M. Abdel-Gaber, H. T. Rahal and F. T. Beqai, Eucalyptus leaf extract as a eco-friendly corrosion inhibitor for mild steel in sulfuric and phosphoric acid solutions, *Int. J. Ind. Chem.*, 2020, **11**(2), 123–132.
27 A. M. Abdel-Gaber, R. Awad, H. T. Rahal and D. Moussa, Electrochemical behavior of composite nanoparticles on the corrosion of mild steel in different media, *J. Bio-Tribo-Corrosion*, 2019, **5**(2), 49.
28 A. M. Abdel-Gaber, H. T. Rahal, N. Thebian and G. Younes, Experimental and theoretical chemical studies of linalool and caffeine as corrosion inhibitors for mild steel in sulfuric acid solutions, *Biointerface Res. Appl. Chem.*, 2024, **14**(1), 1–2.
29 S. Z. Salleh, A. H. Yusoff, S. K. Zakaria, M. A. Taib, A. A. Seman, M. N. Masri, M. Mohamad, S. Mamat, S. A. Sobri, A. Ali and P. Ter Teo, Plant extracts as green corrosion inhibitor for ferrous metal alloys: a review, *J. Cleaner Prod.*, 2021, **304**, 127030.
30 N. Chaubey, A. Qurashi, D. S. Chauhan and M. A. Quraishi, Frontiers and advances in green and sustainable inhibitors for corrosion applications: a critical review, *J. Mol. Liq.*, 2021, **321**, 114385.
31 S. H. Alrefaee, K. Y. Rhee, C. Verma, M. A. Quraishi and E. E. Ebenso, Challenges and advantages of using plant extract as inhibitors in modern corrosion inhibition systems: recent advancements, *J. Mol. Liq.*, 2021, **321**, 114666.
32 A. Singh, M. Chaudhary, M. Verma, N. Kaur and N. Singh, Chaotropic anion induced self-assembly of naphthalimide–glutathione nanohybrids: selective recognition of bisulphate anions in aqueous medium, *New J. Chem.*, 2023, **47**(48), 22430–22440.
33 R. Attri, A. Singh, J. Kaur, G. Singh, A. Saxena, M. Khalid and G. S. Albakri, Sustainable carbon quantum dots–chitosan hydrogel composite for corrosion protection of mild steel in 1 M sulfuric acid, *Int. J. Biol. Macromol.*, 2025, 146391.
34 B. Kallauraya, R. S. Bhat, S. I. Bhat, V. Kamat, M. Akki, A. Kumar, K. Jyothi and B. R. Bharat, Synthesis, characterization, and evaluation of pyrimidinone-linked thiazoles: DFT analysis, molecular docking, corrosion inhibition, and bioactivity studies, *Heliyon*, 2024, **10**(20), e39421.
35 A. H. Alamri, K. Rasheeda, S. J. Kamal, M. Aljohani, T. A. Aljohani, I. Baig, V. D. Alva, N. P. Swathi, I. B. Onyeachu and S. Samshuddin, Pyrimidine derivatives as efficient anticorrosive agents for acid corrosion of mild steel: electrochemical and computational validation, *Arabian J. Chem.*, 2024, **17**(6), 105752.
36 J. Haque, C. Verma, V. Srivastava, M. A. Quraishi and E. E. Ebenso, Experimental and quantum chemical studies of functionalized tetrahydropyridines as corrosion inhibitors for mild steel in 1 M hydrochloric acid, *Results Phys.*, 2018, **9**, 1481–1493.
37 K. Rasheeda, A. H. Alamri, P. A. Krishnaprasad, N. P. Swathi, V. D. Alva and T. A. Aljohani, Efficiency of a pyrimidine derivative for the corrosion inhibition of C1018 carbon steel in aqueous acidic medium: experimental and theoretical approach, *Colloids Surf., A*, 2022, **642**, 128631.
38 I. B. Onyeachu, D. S. Chauhan, M. A. Quraishi, I. B. Obot and A. Singh, (*E*)-2-amino-7-hydroxy-4-styrylquinoline-3-carbonitrile as a novel inhibitor for oil and gas industry: influence of temperature and synergistic agent, *J. Adhes. Sci. Technol.*, 2022, **36**(17), 1858–1882.
39 I. Arshad, K. Qureshi, A. S. Saleemi, A. Abdullah, A. A. Bahajjaj, S. Ali and A. Bokhari, Melamine–isatin tris Schiff base as an efficient corrosion inhibitor for mild steel in 0.5 molar hydrochloric acid solution: weight loss, electrochemical and surface studies, *RSC Adv.*, 2023, **13**(28), 19301–19311.
40 H. T. Rahal, A. M. Abdel-Gaber and G. O. Younes, Inhibition of steel corrosion in nitric acid by sulfur containing compounds, *Chem. Eng. Commun.*, 2016, **203**(4), 435–445.
41 M. Errili, K. Tassaoui, A. Chraka, M. Damej, H. T. Rahal, N. Labjar, A. El Mahmoudi, K. Bougrin, A. Berisha and

M. Benmessaoud, Synthesis and investigation of novel sulfonamide-1,2,3-triazoles corrosion inhibitors for E24 steel in 1 M HCl solution: a combination of modeling and experimental approaches, *Int. J. Corros. Scale Inhib.*, 2024, **13**(3), 1607–1635.

42 S. Ksama, K. Tassaoui, A. Chraka, K. Chkirate, M. Damej, N. Ouadghiri, M. Errili, K. Azgaou, E. M. Essassi, H. T. Rahal and M. Benmessaoud, Detailed experimental and computation/molecular simulation of 1,5-benzodiazepin derivative as corrosion inhibitor for E24 steel in 1 M HCl environment, *Int. J. Corros. Scale Inhib.*, 2024, **13**(4), 2054–2086.

43 F. Ennafaa, A. Chraka, K. Tassaoui, I. Mouamr, M. Damej, A. E. Mahmoudi, K. Bougrin, H. T. Rahal and M. Benmessaoud, An experimental and dual computational study using DFT and MD simulations to better understand the adsorption and corrosion-inhibiting properties of *N*-(3-(4-methoxyphenyl) isoxazol-5-yl) methyl saccharin for C38 Steel in acidic medium, *Mater. Chem. Phys.*, 2025, **334**, 130441.

44 F. Benhiba, R. Hsissou, K. Abderrahim, H. Serrar, Z. Rouifi, S. Boukhris, G. Kaichouh, A. Bellaouchou, A. Guenbour, H. Oudda and I. Warad, Development of new pyrimidine derivative inhibitor for mild steel corrosion in acid medium, *J. Bio-Tribo-Corrosion*, 2022, **8**(2), 36.

45 T. Aravinda, D. Kumari, A. S. Sowmyashree, S. Rao, K. J. Gururaj, P. Naik and G. Nagendra, Fmoc Centred Peptide Conjugate as an Effective Corrosion Inhibitor for Mild Steel in Acidic Medium: A Combined Theoretical and Experimental Approach, *Mater. Today Commun.*, 2025, 113142.

46 M. Oubaaqa, M. Ouakki, M. Rbaa, A. Elgendy, R. Idouhli, M. Maatallah, A. Jarid, M. E. Touhami, B. Lakhrissi and A. Zarrouk, Two pyran derivatives as corrosion inhibitors for mild steel in HCl solution: experimental and theoretical investigations, *Mater. Today Commun.*, 2023, **35**, 106188.

47 S. Guo, J. An, Z. Dong, J. Tao, J. Cheng, J. Wu and C. Dong, Two nicotinic acid-amino acid derivatives as green corrosion inhibitors for Q235 steel in 1 M HCl solution, *Mater. Today Commun.*, 2025, **43**, 111661.

48 Y. Youssefi, M. Jabha, L. Oucheikh, O. Ou-ani, H. Lgaz, A. Hasnaoui, A. Oubair, M. Znini, H. S. Lee and B. Hammouti, Evaluating corrosion inhibition of spiro-pyrazoline-butyrolactones on carbon steel in HCl: experimental, computational, and COSMO-RS approaches, *Mater. Today Commun.*, 2025, **44**, 111800.

49 N. Idlahoussaine, W. Daoudi, B. El Ibrahimi, E. Berdimurodov, M. Lasri, R. Idouhli, M. El Ouardi, N. Aliev, A. El Aatiaoui, A. Abouelfida and A. Ait Addi, The application of 2-(3-nitrophenyl)imidazo[1,2-α]pyridine as an effective corrosion-defender for steel in acidic environment, *Mater. Today Commun.*, 2024, **40**, 109695.